Molecular Modeling of the Flexible Cell Wall Polysaccharide of *Streptococcus mitis* J22 on the Basis of Heteronuclear NMR Coupling Constants†

Qiuwei Xu and C. Allen Bush*

Department of Chemistry and Biochemistry, University of Maryland−Baltimore County, Baltimore, Maryland 21228

Received May 28, 1996; Revised Manuscript Received August 30, 1996⊗

ABSTRACT: A method for constructing conformational models of flexible complex polysaccharides on the basis of NMR data and molecular modeling is described and is applied to a polysaccharide which is a lectin-binding receptor important in coaggregation of oral bacteria. The method involves uniform biosynthetic enrichment of the polysaccharide with ^{13}C which allows accurate measurements of heteronuclear coupling constants from a three-dimensional coupled HMQC-NOESY spectrum. The improved resolution of the 3D spectrum also provides a large number of accurate values of NOE cross peak volumes in a decoupled HMQC-NOESY spectrum. While it was not possible to construct a model for the flexible polysaccharide directly from the NOE data, a model was successfully built from the coupling constant data. Possible values of glycosidic dihedral angles were extracted from the $^3J_{CH}$ data to build models which were evaluated by molecular modeling calculations. A simple average over a linear combination of low-energy conformations was selected which matched the experimental $^3J_{CH}$ data within experimental error. Simulation of the NOE data for this same combination of conformers gave excellent agreement with experimental NOESY data. Molecular dynamics trajectories both with and without coupling constant constraints do not represent the experimental NOE and $^3J_{CH}$ data as well as the linear combination model. While the polysaccharide has some flexibility in the antigenic site, the lectin-binding site, which contains a furanoside with (1→6)-linkages, provides a more flexible hinge in the polysaccharide.

A number of strains of oral *Streptococci* have been identified which coaggregate specifically both with other streptococcal species and with representatives of other genera such as actinomyces (Kolenbrander & London, 1993). These coaggregations between strains which are known to be early colonizers of the freshly cleaned tooth surface are thought to play an important role in the first stages of formation of dental plaque. Many of these coaggregations are inhibited by sugars and there is considerable evidence that the species specificity of the coaggregation results from interaction of a lectin on the surface of one cell with a cell surface polysaccharide on the coaggregation partner.

Our research group has participated in studies of the chemical structure of the cell wall polysaccharides of *Streptococcus mitis* J22 (Abeygunawardana et al., 1990) as well as of a number of other *Streptococci* (Abeygunawardana & Bush, 1993; Reddy et al., 1993). These studies have resulted in the identification of two distinct carbohydrate epitopes in these polysaccharides, one which is the receptor for lectin binding and the other which is the antigenic epitope (Cisar et al., 1995). The complete chemical structure of the cell wall polysaccharide of *S. mitis* J22 was found to contain seven sugar residues in the repeating unit which are linked through phosphate diester bonds as shown in Chart 1.

The lectin-binding site is associated with residues **d**, **e**, and **f** while residues **a**, **b**, **c**, and **g** make up the antigenic site. All the sugar residues are of the D configuration except for the two rhamoses, which are L.

Cassels et al. (1995) have reported molecular modeling studies of this polysaccharide and have proposed a model

Chart 1: *S. mitis* J22 Polysaccharide (Proposed Lectin-Combining Site Is Underlined.)

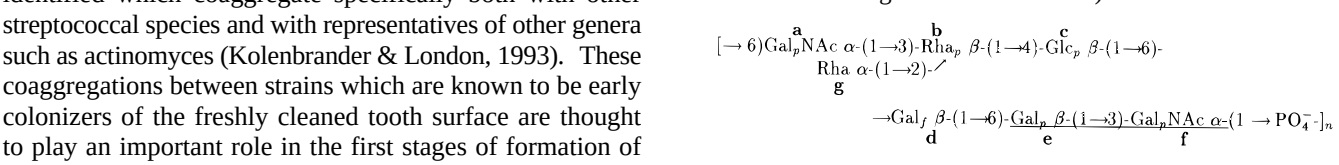

in which strong hydrogen bonding interactions contribute to a folded structure. Our group has reported molecular modeling and NMR[1] data on the conformation of antigenic tetrasaccharide site which indicated that the polymer is highly flexible with no single conformation which is consistent with the experimental data (Xu et al., 1996a). The model proposed in our work features three conformers which coexist in solution in fast exchange on the NMR chemical shift time scale. Subsequent NOE studies on the conformation of a heptasaccharide isolated from the polysaccharide were found to be consistent with the model for the polymer (Xu et al., 1996b). This result indicates NOE intensities from the polymer and oligomer can both be accounted for with the same combination of conformations based on a simple isotropic model. Therefore we have concluded that effects of anisotropic motion are not likely to be significant for interpretation of NOE of the polysaccharide.

Most lectin−carbohydrate interactions are relatively weak with the dissociation constant in the high micromolar to millimolar range for binding of a single carbohydrate epitope

† Research supported by NSF Grant DMB-91-05586.
⊗ Abstract published in *Advance ACS Abstracts,* November 1, 1996.

[1] Abbreviations: NMR, nuclear magnetic resonance; NOE, nuclear Overhauser effect; HMQC, heteronuclear multiple quantum coherence; NOESY, nuclear Overhauser effect spectroscopy; TOCSY, total correlation spectroscopy; RF, radio frequency; FID, free induction decay; MD, molecular dynamics; r-MD, restrained molecular dynamics; tar-MD, time-averaged restrained molecular dynamics.

S0006-2960(96)01262-7 CCC: $12.00

by the lectin. For such weak interactions to give rise to the observed interactions between cells, the binding must be cooperative with multiple lectin-binding epitopes of the polysaccharide on the surface of one cell binding to multiple lectin-binding sites on the partner cell. Cooperative interactions of this type are important in many other biological phenomena. As a result of the cooperativity, the binding depends not only on conformation of the binding epitope itself but also on the conformation and dynamics of the links between the lectin-binding sites. The conformation of small oligosaccharide lectin-binding epitopes has been extensively studied. The results and the significance of flexibility of lectin-binding sites on the thermodynamics of binding have been discussed in numerous reviews (Carver, 1993; Bush, 1992; Homans, 1993), but the flexibility of the entire polymer including the dynamics and conformation of the polysaccharide parts which link the lectin-binding epitopes together has received less attention.

There has been the considerable discussion in the literature about the structural factors of oligosaccharides which influence flexibility. In general, the crowded stereochemistry of glycosidic linkages leaves a rather limited amount of conformational space available and a conformational map for a disaccharide often shows only a few minimum energy conformations. However, it is clear that in some types of disaccharide linkage there are several accessible conformations conferring flexibility (Rice et al., 1993). It appears that there are some comparatively rigid epitopes, such as those of the blood group oligosaccharides. For these types of oligosaccharides, it is possible to construct a simple conformational model based on NOE data and molecular modeling (Miller et al., 1992). In our group we have used an NOE mapping procedure originally proposed by Brisson and Carver (1983) which can be adapted to NOESY data (Bush, 1994). But other procedures have been used to find the conformations of relatively rigid oligosaccharides, including restrained molecular dynamics simulation (Rutherford et al., 1995). On the other hand, many oligosaccharides are comparatively flexible, with two or more distinct conformations in exchange. For those cases, it can be shown that no single conformation will fit the NOE data (Cumming & Carver, 1987; Poppe & van Halbeek, 1992; Poppe et al., 1994; Lommerse et al., 1995; Xu et al., 1996a,b).

While it is possible with the NOE and molecular modeling methods to show that an oligosaccharide is not rigid, it has proven to be considerably more difficult to construct realistic models of flexible oligosaccharides on the basis of NOE data. One approach is the virtual conformation model of Cumming and Carver (1987) in which one that assumes a small number of discrete conformations exchange on time scale which is slow compared to the overall tumbling time. For this model, one calculates average values of the elements of the NOE relaxation matrix, ρ and σ. This procedure accounts for the r^{-6} weighting of dipolar relaxation which strongly weights short proton distances and also accounts for multiple spin relaxation pathways. But it has proven difficult to apply this model directly since the statistical weights of the conformations contributing to the average are not determined with sufficient accuracy by the molecular modeling methods (Rutherford & Homans, 1994; Xu et al., 1996a). An additional uncertainty arises regarding the dynamics of conformational exchange which may not fit the assumptions of this model. The kinetics of conformational exchange in oligosaccharides which are complex and not well understood may not be much slower than tumbling rates (Hricovini et al., 1992). Lommerse et al. (1995) have discussed models for calculation of NOE averaged over multiple conformations of oligosaccharides for which internal motions are fast compared to the tumbling time. The number of parameters needed to define such models is much greater than the experimental data available, requiring either severe approximations or heavy reliance on molecular dynamics simulations for which the detailed reliability can be questioned.

Bonvin and Brunger (1996) have addressed the question of whether it is even possible to deduce conformations of flexible biopolymers from NOE data. They conclude that construction of models for flexible molecules will require additional experimental data to define the different contributing conformations and their statistical weights. A possible source of additional data for oligosaccharides is long-range heteronuclear coupling constants across the glycosidic linkage which can be correlated with glycosidic dihedral angle (Hamer et al., 1978). An advantage of the coupling data is that the measured parameter, $^3J_{CH}$, is correlated directly with the key internal coordinate that determines conformation, the glycosidic dihedral angle. An additional advantage for molecules in conformational exchange is that the appropriate time scale for averaging of coupling constants is more certain than for NOE. Since conformational exchange is certainly fast on the time scale of milliseconds, a simple average over the conformations is appropriate.

There have been several problems preventing extensive use of $^3J_{CH}$ data in determining oligosaccharide conformations. The primary problem is the difficulty of accurate measurements. But the measurement of coupling constants has been facilitated recently by the development of NMR techniques to accurately measure heteronuclear coupling constants (Zhu et al., 1994; Biamonti et al., 1994). We have recently reported $^3J_{CH}$ data in oligosaccharides and polysaccharides which have been carefully checked against reliable values measured for model compounds (Gitti et al., 1994; Xu et al., 1996b). The availability of polysaccharides with uniform enrichment in ^{13}C greatly facilitates these measurements. The interpretation of the data requires a precise correlation of $^3J_{CH}$ with glycosidic dihedral angle. Although detailed correlation functions have been proposed (Mulloy et al.,1988; Tvaroska et al., 1989), their accuracy has been criticized since they fail to account for the positions of electronegative substituents on the coupling pathway (Podlaske et al., 1995).

In this paper we report measurements of all the relevant coupling constants for a ^{13}C-enriched bacterial polysaccharide from *S. mitis* J22 by a ^{13}C-resolved 3D NOESY method. We show that the coupling data can be incorporated in molecular modeling calculations to derive a flexible model for the heptasaccharide repeating unit of the polymer. We also report extensive NOE data for the labeled polymer derived from decoupled 3D ^{13}C resolved HMQC-NOESY spectra and we show that the NOE data fit the flexible model derived from the coupling data. We will also report in a separate paper heteronuclear ^{13}C relaxation data showing internal motions both on the picosecond time scale and on the nanosecond time scale which can be reconciled with our molecular model [Xu & Bush, 1996 (accompanying paper)].

MATERIALS AND METHODS

NMR

The polysaccharide sample from *S. mitis* J22 was ^{13}C enriched to 96% according to the procedure described previously (Gitti et al., 1994). The sample was dissolved in 99.96% D_2O at a concentration of 7−10 mg/mL at neutral pH without any buffer.

^1H-decoupled 3D HMQC-NOESY spectra were acquired on a GN-500 NMR instrument with a pulse sequence based on that described by Fesik and Zuiderweg (1988). A delay of 3.4 ms was employed in the HMQC part to develop the heteronuclear anti-phase magnetization, and the mixing time was 350 ms. The spectral width of the proton dimensions (t_2 and t_3) was 2500 Hz. The acquisition dimension (t_3) contains 512 complex data points with eight transients. The evolution ^1H dimension (t_2) was obtained by acquiring 64 complex 2D planes. The ^{13}C pulses were applied through the f_3 channel with carrier frequency in the middle of saccharide anomeric and ring ^{13}C region with spectrum width of 13 158 Hz. Therefore, methyl carbons were folded into the downfield side of the ^{13}C dimension. The ^{13}C evolution dimension was obtained by acquiring 64 complex blocks. The decoupling of ^{13}C along acquisition dimension (t_3) was accomplished through WALTZ-16 with a decoupling RF field strength of 4.0 kHz, and ^{13}C decoupling along t_2 was realized with a ^{13}C composite 180° pulse in the middle of proton evolution period (t_1). The total acquisition time was about 64 h for this 3D experiment.

$^1H-^{13}C$ coupled 3D HMQC-NOESY was carried out on a GE-Omega 500 spectrometer using a pulse sequence based on that described by Fesik and Zuiderweg (1988). Since there was no ^{13}C decoupling during proton evolution and acquisition periods, proton peaks doubled along each proton dimension due to coupling to their bonded ^{13}C. The NOE mixing time was 200 ms. The spectral width for the proton dimensions (t_2 and t_3) was 2500 Hz. The acquisition dimension (t_3) contained 512 complex data points with eight transients. The evolution ^1H dimension was obtained by acquiring 64 complex 2D planes. The spectral width of ^{13}C was 14 493 Hz with 64 complex blocks.

Felix 2.05 software was used to process the 3D HMQC-NOESY data. 3D matrices of 1024 × 128 × 1024 ($t_3 \times t_1 \times t_2$) were generated in real data type. Linear prediction was used for the first point of FID's along the ^{13}C evolution dimension to provide a flat base line along the ^{13}C dimension of the spectrum. FID's along the two evolution dimensions (t_1 and t_2) were extended from 64 points to 128 points with linear prediction before apodization with a cosine bell function. FID's along the ^1H evolution dimension were zero filled to 1K data points. Fourier transformation was applied to each dimension followed by phase correction. The base lines along the two proton dimensions were flat and needed no further smoothing. All the cross peaks in 3D spectra were assigned according to previously reported chemical shift data (Abeygunawardana et al., 1990). Each cross peak area on NOESY planes was picked out manually and integrated with the Felix software according to assigned peak area.

Heteronuclear coupled HMQC-NOESY was processed with Felix 2.30 software (Biosym) on an SGI workstation. The data along proton and carbon dimensions were zero-filled to 1024 points and 128 points, respectively, with linear prediction for the first point of each FID along the ^{13}C dimension. All the FID's were apodized with a cosine bell function before Fourier transformation. All the cross peaks in heteronuclear-coupled HMQC-NOESY were assigned by matching chemical shifts of middle points of 13-coupled protons and previously assigned data. The $^3J_{CH}$ values were obtained from NOESY by a shift and match scheme as in E.COSY. On a NOESY plane of carbon labeling C*x*, two sets of row vectors containing cross peaks of H*x* and H*y* were selected and the vectors were truncated to contain only the cross peak of interest (H*x*/H*y*). After reverse Fourier transformation, the new time domain data were zero filled and Fourier transformed with a resolution of 0.32 Hz. The two new vectors were saved in ASCII. Their amplitudes and frequencies were matched with a self-coded program based on the singular value decomposition method (SVD) (Press et al., 1992). The frequency shift which gave minimum root mean square difference for the above SVD match of the two vectors is the long-range heteronuclear coupling constant, $^3J_{CH}$.

Modeling

Molecular modeling for the polysaccharide was done with CHARMm version 22 (Polygen). The force field parameters were those of Polygen which are based on CHARMm parameters as modified for carbohydrates by Ha et al. (1988). The residue topology file (RTF) was modified to include L-rhamnose for which charges were assigned from fucose. It was also necessary to add β-galactofuranose to the RTF which was based on α-arabinofuranose.

The dielectric constant was set as distance dependent (RDIE) in these calculations. The nonbonded interaction energy (van der Waals and electrostatic energy) was calculated with a smooth-switch function (Brooks et al., 1983) with a cutoff distance of 15.0 Å. A visual check on conformations was carried out with the QUANTA molecular graphics software (Biosym).

Starting conformations for molecular modeling of the heptasaccharide subunit of the polysaccharide were selected as follows. The dihedral angles across the glycosidic linkages of the segment, **a-b(-g)-c**, were taken from the previously established conformation for this antigenic site (Xu et al., 1996a). The remaining dihedral angles across the glycosidic linkages for the repeating heptasaccharide were selected to give reasonable starting conformations based on $^3J_{CH}$ data as discussed below. Selected conformations were then energy minimized with 300 steps of steepest descent followed by 500 steps of conjugate gradient minimization.

None of these individual starting conformations for this flexible polysaccharide was adequate to model the experimental NMR data. Therefore, linear combinations of individual starting conformations were sought which would reproduce the experimental $^3J_{CH}$ data and eventually the NOE data as well. The search was based on a linear combination of $^3J_{CH}$ values of individual models using the SVD method (Press et al., 1992).

$$^3J^{\,o}_{CH} = \sum_i p_i \times {}^3J^{\,c}_{CH_i} \qquad (1)$$

where $\sum_i p_i = 1$ and p_i is a statistical weight of conformer *i*. $^3J^{\,o}_{CH}$ refers to observed experimental value of the coupling constant, and $^3J^{\,c}_{CH_i}$ refers to the values calculated from a

single conformation of the model. ${}^3J^{\,c}_{CH_i}$ was calculated with the following equation (Tvaroska et al., 1989)

$$ {}^3J^{\,c}_{CH_i} = 5.7\cos^2(\theta) - 0.6\cos(\theta) + 0.5 \qquad (2) $$

where $\theta = \Phi_H$ is defined by the four atoms, H1-C1-O-C*x*, or Ψ_H is defined by the four atoms, C1-O-C*x*-H*x*. According to the IUPAC-approved definition, the glycosidic dihedral angle Φ is defined by O5-C1-O-C*x*(O4-C1-O-C*x* for furanose) and Ψ is defined by C1-O-C*x*-C*x*−1. The two definitions are correlated depending on the configuration at C1 or C*x*. For example, the relationship $\Phi \approx \Phi_H + 120°$ holds for an α-(1→4)-linkage of a D sugar, and $\Phi \approx \Phi_H - 120°$ for a β-(1→4)-linkage of a D sugar. For (1→6)-linkages, an additional dihedral angle ω is defined by the four atoms O6-C6-C5-O5. For the (1→6)-linked galactofuranose residue, an additional conformational dihedral angle, γ, is defined by the four atoms C6-C5-C4-O4 in addition to ω for the (1→6)-linkage.

The pucker of the galactofuranose residue **d** is described by a single variable called the phase angle, *P*. It is defined as (Saenger, 1983)

$$ \tan P = \{(\nu_4 + \nu_1) - (\nu_3 + \nu_0)\}/\{2\nu_2(\sin 36° + \sin 72°)\} \qquad (3) $$

In this equation, ν_0 is defined by the four atoms C4-O4-C1-C2, ν_1 is defined by O4-C1-C2-C3, ν_2 is defined by C1-C2-C3-C4, ν_3 is defined by C2-C3-C4-O4, and ν_4 is defined by C3-C4-O4-C1.

The statistical weights, p_i, extracted from eq 1 by the method described above were used to calculate the expected NOE for the model for comparison with experimental data. For this purpose, the "virtual conformation" model was used in which the NOESY relaxation rate matrix elements were weighted and the average matrix was used to calculate the NOE for the model (Keepers & James, 1984; Borgias & James, 1989). The quality of simulated NOE intensities was judged by calculating the crystallographic-type *R*-factor and sixth-root weighted R^x factor (James, 1991):

$$ R = \{\sum_i |I^{\,o}_i - I^{\,c}_i|\}/\{\sum_i I^{\,o}_i\} \qquad (4) $$

$$ R^x = \{\sum_i |(I^{\,o}_i)^{1/6} - (I^{\,c}_i)^{1/6}|\}/\{\sum_i (I^{\,o}_i)^{1/6}\} \qquad (5) $$

In these equations, $I^{\,o}_i$ and $I^{\,c}_i$ refer to the observed and calculated NOE magnitudes, respectively.

In order to probe the dynamics of this flexible polysaccharide and for mapping the dihedral angle space accessible to those multiple conformers, dynamics simulation was run for the conformers derived from the best ${}^3J_{CH}$ data fitting. Dynamics simulations were run both with and without dihedral angle constraints derived from the experimental coupling constants. The constraint for ${}^3J_{CH}$ was constructed as a parabolic function (Mierke et al., 1994; Eberstadt et al., 1995).

$$ E_{J,i} = 0.5 \times K_J\,({}^3J^{\,c}_{CH_i} - {}^3J^{\,o}_{CH_i})^2 \qquad (6) $$

In this equation, ${}^3J^{\,o}_{CH_i}$ is an observed ${}^3J_{CH}$ value and ${}^3J^{\,c}_{CH_i}$ is a calculated value from the model with eq 2. The force constant K_J of the constraint was set as 1.0 kcal/mol Hz^2.

Table 1: Experimental and Calculated ${}^3J_{CH}$ of Polysaccharide of *S. mitis* J22 (in Hz)

	calcd[a]	exptl		calcd	exptl
${}^3J_{CH(\Phi H)ab}$	1.70	1.50	${}^3J_{CH(\Psi H)ab}$	2.31	1.50
${}^3J_{CH(\Phi H)bc}$	1.73	2.00	${}^3J_{CH(\Psi H)bc}$	2.10	2.10
${}^3J_{CH(\Phi H)gb}$	1.48	1.50	${}^3J_{CH(\Psi H)gb}$	3.39	4.10
${}^3J_{CH(\Phi H)cd}$	1.46	1.50	${}^3J_{CH(\Psi H)cd}$	2.18	1.90
${}^3J_{CH(\Phi H)de}$	2.04	1.50	${}^3J_{CH(\Psi H)de}$	1.40	1.30
${}^3J_{CH(\Phi H)ef}$	2.71	2.40	${}^3J_{CH(\Psi H)ef}$	2.36	1.30
		$\sigma = 0.50$ Hz[b]			

[a] ${}^3J_{CH}$ calculated from statistical weights of Table 5 and the dihedral angle correlation of Tvavoska et al. (1989). [b] σ is the standard deviation between calculated and experimental ${}^3J_{CH}$.

The atomic force from the above penalty function (eqs 2 and 6) required for molecular dynamics simulation is obtained from the partial derivatives (Mierke et al., 1994; Eberstadt et al., 1995)

$$ F_{J,i} = -\partial E_{J,i}/\partial r_i = -(E_{J,i}/\partial J)(\partial J/\partial\theta)(\partial\theta/\partial r_i) \qquad (7) $$

where r_i is the distance between C and H. The penalty energy and atomic force was incorporated in the "user subroutines" in the CHARMm source codes.

The dynamics simulation was carried out in vacuum. All the bonds with hydrogens were constrained with SHAKE using 1×10^{-10} tolerance. The energies of the starting conformers were minimized with 200 steps of steepest descent followed by 200 steps of conjugate gradient minimization, and then the conformer was heated from 0 to 300 K in 3 ps steps with a 5 K increment. The conformer was later equilibrated at 300 K for 1 ps before 1.0 ns dynamic simulation. The Verlet algorithm was used to compute the molecular dynamics trajectories. The constrained dynamics simulation at 300 K was run with a constant temperature method at an equilibrium rate of every 5 fs with a coupling decay time of 0.001 ps.

RESULTS AND DISCUSSION

The long-range heteronuclear coupling constants ${}^3J_{CH}$ across the glycosidic linkages of this polysaccharide obtained from the 3D ${}^1H-{}^{13}C$-coupled HMQC-NOESY spectrum are given in Table 1. It is somewhat surprising that 11 out of the 12 ${}^3J_{CH}$ values are small (~2 Hz), but the method used has been carefully validated. ${}^nJ_{CH}$ values within individual pyranoside rings measured from 2D NOESY and TOCSY spectra were compared with known values for model monosaccharides showing experimental error of ±0.5 Hz (Gitti et al., 1994). The 3D method used in this work gives spectra which look similar to the figures reported by Gitti et al. (1994), and all of the ${}^3J_{CH}$ values reported here are identical to those reported in the earlier work. The advantage of the 3D method is that the improved resolution eliminates much of the overlap which has a very deleterious effect on measurements of ${}^nJ_{CH}$ by this method.

In the ${}^{13}C$-decoupled NOESY spectrum, cross peak volumes are related to proton proximities providing additional information on the polysaccharide conformation. 2D NOESY spectra of the polysaccharide provide a few cross peaks across the glycosidic linkages, but many interresidue cross peaks overlap because ring protons tend to appear within a 1 ppm chemical shift region. The NOESY cross peak separation along the carbon dimension in 3D HMQC-

Table 2: ^{13}C-Enriched Polysaccharide of J22 with 350 ms Mixing at 24.0 °C

cross-peaks	calcd intensity[a]	exptl intensity	cross-peak	calcd intensity	exptl intensity
aH1-bH1	0.0053	0.0052	bH5-cH2	0.0007	0.0070
aH1-bH2	0.0488	0.0340	gH2-cH2	0.0001	0.0003
aH1-bH3	0.0237	0.0159	gH2-cH5	0.0004	0.0019
aH1-bH4	0.0030	0.0051	gH3-cH5	0.0042	0.0004
aH1-bH5	0.0019	0.0010	gH5-cH5	0.0169	0.0081
aH1-gH1	0.0285	0.0130	cH1-dH6	0.0301	0.0313
aH1-gH4	0.0007	0.0008	cH1-dH6′	0.0240	0.0226
aH1-gH5	0.0040	0.0017	cH1-dH5	0.0040	0.0143
aH2-bH1	0.0006	0.0005	cH1-dH4	0.0046	0.0069
aH2-bH2	0.0050	0.0062	cH2-gH2	0.0001	0.0003
aH2-bH3	0.0031	0.0018	cH2-dH6	0.0019	0.0015
aH2-gH1	0.0050	0.0038	cH2-dH6′	0.0020	0.0023
aH2-gH5	0.0005	0.0020	cH2-dH5	0.0006	0.0022
aH3-bH3	0.0032	0.0037	cH2-dH4	0.0018	0.0020
aH3-bH1	0.0019	0.0011	cH2-eH3	0.0001	0.0037
aH3-gH1	0.0144	0.0063	dH5-fH5	0.0001	0.0010
aH4-bH3	0.0033	0.0051	dH4-dH1	0.0038	0.0026
aH5-bH1	0.0035	0.0023	dH4-eH5	0.0013	0.0006
aH5-bH3	0.0374	0.0256	dH4-fH5	0.0012	0.0094
aH5-bH4	0.0127	0.0033	dH1-dH2	0.0289	0.0147
aH5-bH5	0.0032	0.0014	dH1-dH3	0.0035	0.0057
aH5-gH1	0.0081	0.0038	dH5-dH1	0.0016	0.0017
aH6-bH3	0.0025	0.0054	dH1-eH1	0.0005	0.0003
aH6′-bH3	0.0038	0.0045	dH1-eH4	0.0019	0.0035
bH1-cH1	0.0013	0.0019	dH1-eH5	0.0037	0.0035
bH1-cH2	0.0025	0.0079	dH1-eH6	0.0241	0.0129
bH1-cH3	0.0130	0.0197	dH1-eH6′	0.0269	0.0099
bH1-cH4	0.0196	0.0437	dH1-fH4	0.0012	0.0031
bH1-cH5	0.0026	0.0040	dH2-eH4	0.0030	0.0038
bH1-gH1	0.0020	0.0084	dH2-fH2	0.0001	0.0002
bH1-gH5	0.0039	0.0053	dH2-fH4	0.0006	0.0010
bH2-gH1	0.0174	0.0253	dH2-fH5	0.0001	0.0043
bH2-gH5	0.0283	0.0120	eH1-fH2	0.0025	0.0077
bH2-cH1	0.0013	0.0004	eH1-fH3	0.0501	0.0282
bH2-cH3	0.0164	0.0043	eH1-fH4	0.0194	0.0058
bH2-cH4	0.0029	0.0066	eH1-fH5	0.0041	0.0018
bH2-c5H	0.0025	0.0027	eH2-fH3	0.0025	0.0017
bH3-gH1	0.0049	0.0029	eH4-fH3	0.0008	0.0083
bH4-gH1	0.0118	0.0034	eH5-fH3	0.0047	0.0084
bH4-gH2	0.0074	0.0034	eH5-fH4	0.0081	0.0012
bH4-cH2	0.0002	0.0011	eH5-fH2	0.0004	0.0007
$R = 0.01$[b]			$R^x = 0.002$[b]		

[a] NOE are calculated from the statistical weights of Table 5 with an effective correlation time of 1.4 ns. [b] R and R^x are the crystallographic-type R-factor and the sixth-root weighted R^x-factor (James, 1991).

NOESY as discussed above makes peak integration accurate, providing many crucial long-range proton cross peaks. The cross peaks reported in Table 2 are an extension of the data reported previously by Xu et al. (1996a) in a paper which treated the conformation of only the antigenic site of this polysaccharide. Instead of recording 3D HMQC-NOESY buildup curves, the dependence of NOE on mixing time was determined from selective ^{1}H T_1 measurements (Bush, 1994). Assuming the diagonal peaks decay as single exponentials, the isolated diagonal peak intensities at zero mixing time were extrapolated with the measured value of selective proton T_1 as the decay time. For diagonal peaks which overlap, the average value of isolated diagonal peak intensities at zero mixing time is used. The experimental values of cross peak volumes shown in Table 2 are the NOE intensities at 350 ms divided by V_0, the intensity of a diagonal peak at zero mixing time. With this normalization, the experimental data may be compared directly with NOESY simulations using the spin matrix method (Keepers & James, 1984; Bush, 1994).

In order to interpret the NOE and $^3J_{CH}$ data in terms of molecular conformations, computer generated molecular models were built. We have previously reported modeling studies on a fragment of four residues (**a**, **b**, **c**, and **g**) which make up the antigenic site. With the additional experimental data reported in this paper, the modeling is extended to include the complete heptasaccharide repeating unit including the lectin-binding site. The phosphate is not included in the modeling since we lack data which determine the conformation of that linkage. Our recently reported NMR data on a dephosphorylated heptasaccharide indicate that the phosphate does not have a great effect on the conformation (Xu et al., 1996b), and preliminary calculations indicate that the phosphate group neutralized by a H^+ ion exerts little influence on the conformation of the seven residues (data not shown).

Several lines of evidence indicate that the heptasaccharide is likely to be quite flexible. First, the NMR lines for this polysaccharide are relatively narrow, indicating that there must be substantial internal motion. Second, even though the branched structure of the antigenic site might be expected to be somewhat rigid, our previous studies (Xu et al., 1996a) nevertheless suggest that multiple conformations exist. The lectin-binding site, with a furanoside and (1→6)-linkages, is expected to be even more flexible.

Building conformational models for flexible oligomers or polymers is a challenging task for which no clear general solution exists in spite of many efforts devoted to flexible peptides (Bruschweiler et al., 1991) and nucleic acids (Ulyanov et al., 1995; Gonzalez et al., 1995) as well as to carbohydrates (Rutherford & Homans, 1994; deWaard et al., 1992; Brisson et al., 1992; Lommerse et al., 1995). Using NOE intensities as distance constraints for flexible molecules requires careful consideration to avoid physically unrealistic "virtual conformations" (Jardetzky, 1980). The NOE mapping procedure, which is reasonably effective for rigid oligosaccharides, has been shown not to be satisfactory for more flexible molecules (Xu et al., 1996a).

Therefore we have taken a novel strategy to building the model in which the $^3J_{CH}$ values are used to guide the conformational search. We had previously observed that the $^3J_{CH}$ data for the antigenic tetrasaccharide provided a useful source of information which could be easily translated into starting conformations by means of eq 2 (Xu et al., 1996a). Therefore, three conformers of the antigenic site determined in that earlier study were combined with conformations of the remaining residues (**d**, **e**, and **f**) which were consistent with the measured $^3J_{CH}$. The dihedral angle values in the antigenic segment, **a-b(-g)-c**, were taken from conformers 3, 4, and 8 of Xu et al. (1996a), and the remaining glycosidic dihedral angles for the starting heptasaccharide conformations were set at values calculated from the measured values of $^3J_{CH}$ according to the calibration curve of eq 2. Since the relationship between $^3J_{CH}$ and dihedral angles is trigonometric, there are four possible dihedral angle values for each measured $^3J_{CH}$. In addition, because H6 and H6′ of residues **d** and **e** were not specifically assigned as *pro-S* or *pro-R*, it was necessary to set starting conformations with all four possible combinations of these assignments for the two (1→6)-linkages in the heptasaccharide as illustrated in Tables 3 and 4. H6′ is defined as the downfield resonance which is well resolved from H6 (Abeygunawardana et al., 1990). There were 49 152 starting conformers resulting from

Table 3: Number of Conformers before Energy Minimization

H6's assignment on **d** and **e**	conformation family		
	3	4	8
H6*R* on **d** and H6*S* on **e**	233	234	234
H6*R* on **d** and H6*S* on **e**	275	275	275
H6*S* on **d** and H6*R* on **e**	230	230	230
H6*S* on **d** and H6*S* on **e**	271	271	271

Table 4: Number of Conformers after Energy Minimization

H6's assignment on **d** and **e**	conformation family		
	3	4	8
H6*R* on **d** and H6*R* on **e**	134	155	48
H6*R* on **d** and H6*S* on **e**	106	84	70
H6*S* on **d** and H6*R* on **e**	83	53	48
H6*S* on **d** and H6*S* on **e**	103	57	75

Table 5: Statistical Weights of Conformers from Linear $^3J_{CH}$ Fitting

conformer[a]	coefficient p_i
322-7 (Figure 1a)	0.4369
322-48 (Figure 1b)	0.3247
422-82 (Figure 1c)	0.2343
422-239	0.0009
822-71	0.0013
822-182	0.0019

[a] Conformers are defined in Table 6.

combinations of starting dihedral angles. Three more dihedral angles which were not experimentally determined, O4-C4-C5-C6 of residue **d**, C4-C5-C6-O6 of residue **d**, and O5-C5-C6-O6 of residue **e**, were set to values obtained by mapping the energies as a function of these angles from −180° to 180° at 60° intervals. The starting phase angle, *P*, for puckering of galactofuranose is 3°. A summary of those starting conformations is given in Table 3 where conformations are grouped according to the starting conformation of the antigenic site, residues **a-b(-g)-c**, and and further classified according to assumptions of which of the two H6′s is *pro-R* and *pro-S* at the (1→6)-linkages (Table 3). Since many of the starting conformations are based on incorrectly assigned angles, it is expected that severe steric conflicts could occur. Therefore, the energies of all the starting conformations were calculated and the conformations within 2000.0 kcal/mol of the lowest energy conformer were selected for energy minimization.

After energy minimization, the conformers listed in Table 4 within a minimum energy of 20 kcal/mol were selected as the conformation pool for matching with the experimental data, $^3J_{CH}$ and NOE. As might be anticipated for a flexible molecule, no single conformer from this pool matches the $^3J_{CH}$ data and therefore a linear combination of conformations from this pool was sought which could reproduce the $^3J_{CH}$ data. A realistic model for this flexible polysaccharide segment presumably requires many conformations in exchange, but with the limited number of experimental $^3J_{CH}$ data given in in Table 1 we must use a limited number of conformations to avoid an under-determined system. We have chosen the number of conformations as six, a compromise value based on the number of experimentally observed $^3J_{CH}$ in Table 1.

The strategy for selecting from the pool of low-energy conformations in Table 4 is as follows. From the entire pool of conformations, we pick one from each of the three most important conformations of the antigenic site, models 3, 4, and 8 from the study of Xu et al. (1996a). Next are selected combinations of conformations of the remaining residues (**d**, **e**, and **f**) along with combinations of the unknown dihedral angles and the assumptions concerning the assignments for the H6's as indicated in the rows of Table 4.

With the conformation pool shown in Table 4, a selection of six conformers from three families requires at least two billion possible combinatorials for one row in Table 4. In order to obtain the best match in reasonable time, the searching process was carried out by first fixing conformers from family 8 followed by searching conformers from families 3 and 4 to best fit experimental data. Then conformers were fixed from family 3, and conformers from families 4 and 8 were searched to best fit the experimental data. The statistical weights of conformers for each linear combination were obtained with singular value decomposition with the minimization of the root mean square difference of $^3J_{CH}$ between experiment and the model (Press et al., 1992). This strategy lacks rigor in that it does not search all possible combinations of the conformers of Table 4. However, alternative strategies which fixed the conformation of either family 3, 4, or 8 give essentially the same statistical weights of the major conformers if the search time or the number of search steps is made sufficiently long. Elimination of either family 3 or 4 does not satisfactorily reproduce the coupling constants within experimental error, and elimination of family 8 has a less important influence on the fitting.

In the best matching combination of conformers, which is listed with statistical weights in Table 5, both H6 protons (the upfield resonance) were assigned as H6S. The dihedral angles for the the six conformers are listed in Table 6, and conformational models for the three most significant contributing models are shown in Figure 1. The structural data in Table 6 show that the variation in the conformation of the lectin-binding site (residues **d**, **e**, and **f**) is greater than

Table 6: Glycosidic Dihedral Angles of Conformers of Flexible Polysaccharide from *S. mitis* J22

	a-b		**b-c**		**g-b**		**c-d**					**d-e**			**e-f**	
conformer	Φ	Ψ	Φ	Ψ	Φ	Ψ	Φ	Ψ	ω^a	γ^b	P[c]	Φ	Ψ	ω^d	Φ	Ψ
322-7	52.2	71.1	44.9	67.6	−54.8	159.0	−64.7	−176.0	−87.0	65.5	−27.3	−29.7	180.0	−165.0	−68.2	−169.0
322-48	52.9	66.3	49.2	69.8	−59.5	162.0	−49.1	98.5	−81.2	35.8	37.8	−169.0	−174.0	37.3	−80.2	175.0
422-82	82.6	168.0	140.0	62.6	−66.7	154.0	−57.8	−160.0	−79.5	68.0	−42.4	−151.0	−176.0	68.0	−77.8	−158.0
422-239	79.3	160.0	135.0	63.2	−83.4	143.0	−31.2	−65.5	−67.9	172.0	−28.0	−65.2	−93.3	60.9	−85.5	−148.0
822-71	63.1	104.0	88.3	−46.5	−85.8	77.0	−67.3	−139.0	−78.6	65.3	−44.9	−47.6	172.0	170.0	−76.3	−166.0
822-182	61.3	108.0	59.2	−78.4	−86.2	122.0	−3.48	75.6	−79.3	160.0	−29.0	−62.4	−81.3	75.9	−33.8	−149.0

[a] ω = O4-C4-C5-C6 of the residue **d**. [b] γ = C4-C5-C6-O6 of the residue **d**. [c] $\tan P - \{(\nu_4 + \nu_1) - (\nu_3 + \nu_0)\}/\{2\nu_2(\sin 36° + \sin 72°)\}$ where ν_0 = C4-O4-C1-C2, ν_1 = O4-C1-C2-C3, ν_2 = C1-C2-C3-C4, ν_3 = C2-C3-C4-O4, and ν_4 = C3-C4-O4-C1. [d] ω = O5-C5-C6-O6 of the residue **e**.

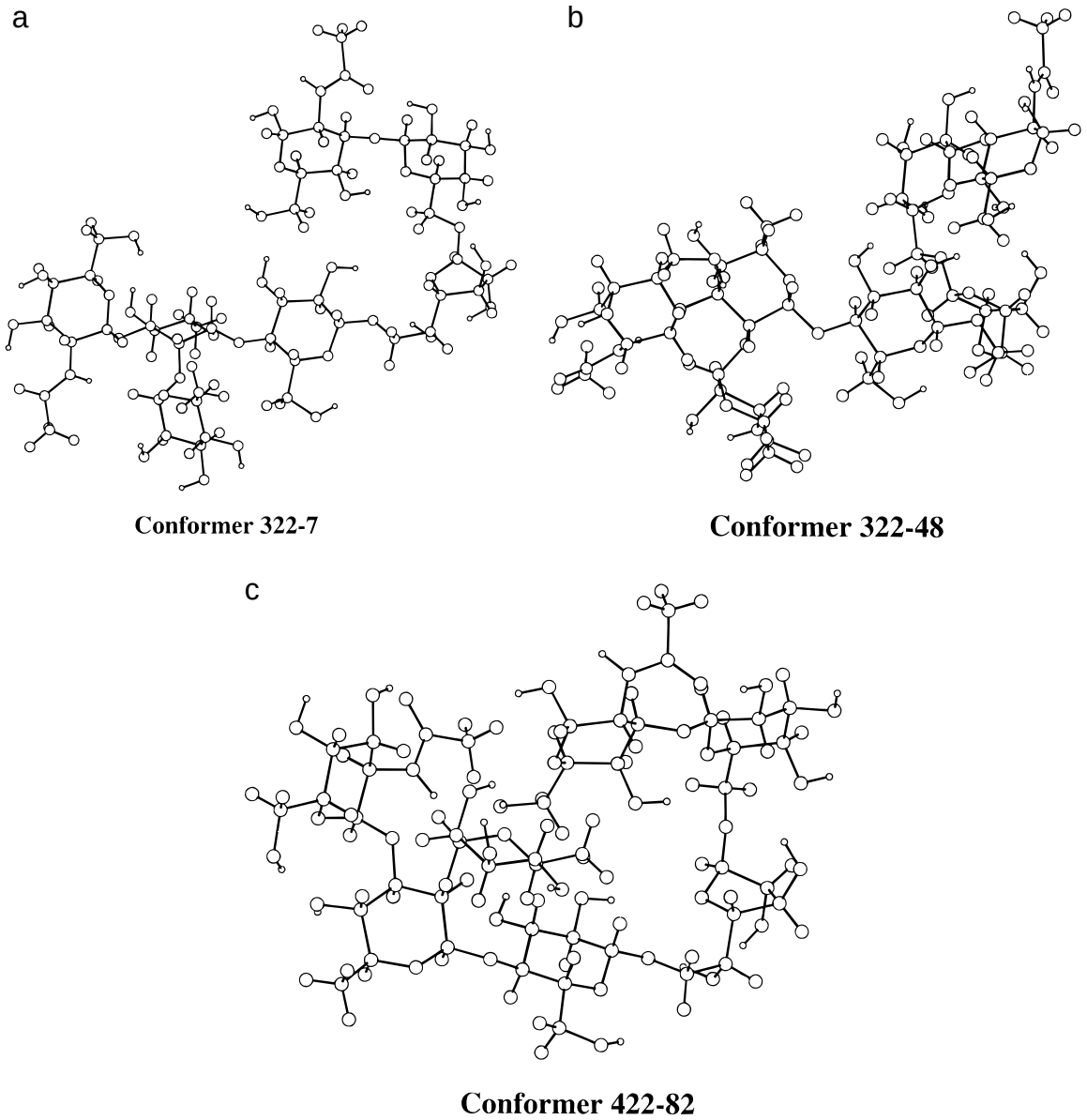

FIGURE 1: Conformational models for three important conformers of Table 6. (a) Conformer 322-7. (b) Conformer 322-48. (c) Conformer 422-82.

that of the antigenic site. Not only does the conformation about the (1→6)-bonds differ, but the galactofuranose puckering as defined by phase angle *P* differs among the conformers redirecting the chain (see Figures 1 and 2.)

While none of the individual conformers in Table 6 can reproduce the experimental $^3J_{CH}$ data of Table 1, the linear combination of these conformers with the statistical weights in Table 5 match experimental results with a root mean square difference between the calculated and experimental data of 0.50 Hz, which is essentially the experimental error of $^3J_{CH}$ measurement. We recognize that a more realistic model of the oligosaccharide subunit should contain more than six conformers in exchange, but the model of Table 5 is adequate to reproduce the experimental data at hand. It also provides an instructive model for interpretation of the NOESY data as well as dynamic data on heteronuclear relaxation rates [Xu & Bush, 1996 (accompanying paper)].

Since this combination of six conformers fits the $^3J_{CH}$ data well, it was necessary to test whether the model could also reproduce the NOESY data. For this purpose, a complete relaxation matrix method was used, in which the average values of the matrix elements were calculated with the statistical weights given in Table 5 (Cumming & Carver, 1987; Bush, 1994). A value of an effective rotational correlation time, which is needed for this method, was taken to be 1.4 ns from our previous work (Xu et al., 1996a). The one-bond $^1H-^{13}C$ dipolar auto-relaxation rate was included in all the diagonal terms of the relaxation matrix. This effect was found to be significant to properly account for the proton auto-relaxation rates for a uniformly ^{13}C-enriched polysaccharide at this effective rotational correlation time. In Table 2, the quality of agreement with experiment of the simulated NOE intensities is evaluated with the two X-ray type indices (R and R^x) as described in Materials and Methods above. The index R reflects the match for short distance NOE data, and R^x reflects the match for long-distance NOE data. Although this model was constructed with $^3J_{CH}$ data and no NOE constraints were used in defining it, nevertheless simulation with this ensemble of conformers is quite satisfactory. The indices of quality are favorable in comparison with results reported for flexible DNA conformations (Ulyanov et al., 1995).

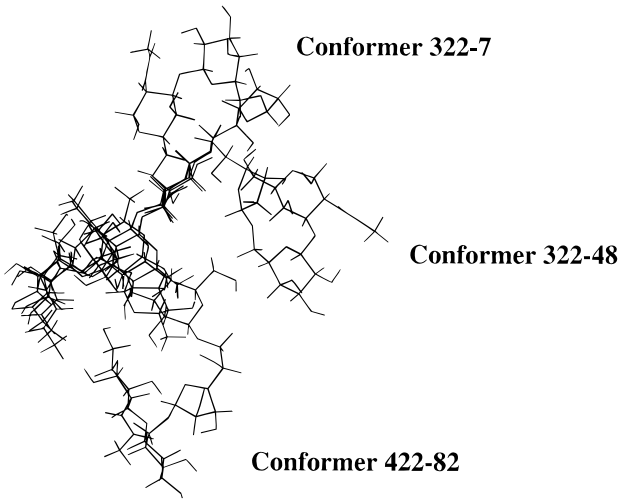

FIGURE 2: Three important conformers of Table 6. Residues **a** and **b** are superimposed for the three conformers as shown on the left side of the figure. The labels of the conformers are at the end of residue **f** on the right side of the figure.

For the model of Table 5, which is based solely on $^3J_{CH}$ data, the statistical weights of conformations from family 8 are negligibly small. Our previous modeling of the antigenic site based on $^3J_{CH}$ data gave only conformers 3 and 4. Conformer 8 was included in that model only to match experimental NOE intensities of the cross peak observed for **b**H1− **c**H5. The statistical weight reported here for conformers from family 8 is based only on $^3J_{CH}$ data with NOE data used only as a check. In fact, the difference between experimental and simulated intensities of the cross peak between **b**H1− **c**H5 in Table 2 is approximately the experimental error of ±0.01, suggesting that a model with only the three major conformers accounts for our data. The phase angle (*P*) of residue **d**, the galactofuranose, varies between −45° and 38°, a region corresponding to the sugar pucker described as C1-*endo*, C2-*exo*, and C3-*endo* for a furanose ring.

A model of the type proposed in Table 5 above based on a linear combination of a small number of distinct conformations can be called a space-averaged model (van Gunsteren et al., 1994). An alternative way of describing a flexible model is the time-averaged method in which a molecular dynamics trajectory is used. Several methods have been described, including free molecular dynamics (MD), restrained molecular dynamics (r-MD), and time-averaged restrained molecular dynamics (tar-MD) (van Gunsteren et al., 1994). MD trajectories of our heptasaccharide model were started from each of the three major conformers of Table 5 and run for 1 ns both as free MD and restrained by $^3J_{CH}$ with constraints of 1.0 kcal/mol Hz^2. A comparison of $^3J_{CH}$ and NOE calculated over these trajectories with experimental results is given in Table S1 in the Supporting Information. In general the values of $^3J_{CH}$ calculated over the free MD trajectories do not agree well with experimental values showing standard deviations of 1.3−1.7 Hz, well outside experimental error. The results for r-MD with $^3J_{CH}$ constraints are considerably better, but still the agreement of calculated values for this time-averaged model is not as good as with the space-averaged model of Table 6. The agreement with experimental data of NOE values calculated from both MD and r-MD is not as good as that with the space-averaged model.

Sample dihedral angle plots from the MD and r-MD trajectories started from each of the three major conformers of Table 5 are shown in Figures S1 and S2 of the Supporting Information. While some transitions are seen among the low-energy conformers, it is obvious that the full conformational space is not sampled uniformly in any of these 1 ns trajectories. In the r-MD simulations, relatively weak constraints were used in an attempt to avoid forcing the trajectories into higher energy virtual conformations. The r-MD trajectories show more limited excursions than the free MD trajectories with a few transitions among local energy minima. The trajectories also show that the lectin-binding site has greater mobility than the antigenic site with significant fluctuations in the furanoside puckering angle and also the dihedral angles ω and γ.

CONCLUSIONS

Although it has been reported that restrained MD simulations using NOE-based constraints leads to a satisfactory model for a large oligosaccharide, the penta-antennary 15-residue N-linked glycopeptide studied by Rutherford et al. (1995) is considerably more rigid than is the polysaccharide from *S. mitis* J22. NOE constraints did not lead to a good model for our polysaccharide while the approach based on $^3J_{CH}$ was successful. Bonvin and Brunger (1996) have proposed that it may not be possible to uniquely and accurately describe flexible biopolymer models from NOE data. We conclude that NOE data are not adequate to determine models for flexible oligosaccharides and that the use of accurately determined $^3J_{CH}$ data across the glycosidic linkage will be extremely valuable for constructing models primarily because of the simplicity of the time averaging of these data compared to the difficulty of averaging NOE data in flexible polysaccharides (Lommerse et al., 1995). We have used $^3J_{CH}$ data to generate starting conformations and also to judge the quality of a flexible model based on exchange among a modest number of distinct conformations. We have shown that molecular modeling constraints in MD simulations based on $^3J_{CH}$ data are also useful for refining structures. The models generated by these procedures fit the NOE data quite well. We conclude that NOE data are not so sensitive to the nature of a flexible model and that their value in describing flexible conformations is much less than their value for describing rigid structures.

We reported results for a space averaged model in which a modest number of conformers was chosen and statistical weights calculated to fit the experiment. While this model is not completely realistic since it does not have enough conformers to fully represent a flexible oligosaccharide, it provides a simple model for the flexible polysaccharide which reproduces both the $^3J_{CH}$ and the NOE data generally better than does the time-averaged model calculated over a 1 ns trajectory. Although it is possible that restrained MD trajectories longer than 1 ns could also provide models which would reproduce both NOE and $^3J_{CH}$ data, detailed interpretations of long trajectories are cumbersome.

Cassels et al. (1995) have reported modeling of the conformation of the polysaccharide from *S. mitis* J22. Although their paper does not quote precise structural parameters, the description of structural features of their model suggests a hairpin bend at the lectin-binding site somewhat similar to our major conformer 322-7 (Table 6

and Figure 1a). But their model does not account for the flexible nature of this polysaccharide which is indicated by our experimental NMR data which include $^3J_{CH}$, NOE, and also ^{13}C relaxation rates (accompanying paper). Their model implies that the residues around the lectin-binding site form a hydrogen-bonded structure with limited internal motion of the dihedral angles of the glycosidic linkages. They also emphasize the role of the phosphodiester linkage in the formation of the folded hydrogen-bonded structure, a feature which is supported neither by our studies on the conformation of the isolated heptasaccharide (Xu et al., 1996b) nor by our calculations.

Our flexible model shows some fluctuation of the antigenic site conformation; we have previously compared data for this tetrasaccharide with those for "rigid" oligosaccharide epitopes such as blood group oligosaccharides (Xu et al., 1996b), but the models of Figure 2 and Table 6 show that there is more variability in the conformation of the lectin-binding site. This result, which is not surprising when one considers the influence of the (1→6)-linkages and the furanoside puckering of residue **d**, is also supported by the MD simulations. In the accompanying paper [Xu & Bush, 1996 (accompanying paper)] we report ^{13}C relaxation data which show that there is a large amplitude of internal motion on the nanosecond time scale in the lectin-binding site.

ACKNOWLEDGMENT

We thank Dr. John O. Cisar of NIDR for continued encouragement and for supplying bacterial strains.

SUPPORTING INFORMATION AVAILABLE

A table and two figures describing the results of free and restrained MD simulations are available along with NOE and $^3J_{CH}$ data computed from them (4 pages). Ordering information is given on any current masthead page.

REFERENCES

Abeygunawardana, C., & Bush, C. A. (1993) *Adv. Biophys. Chem. 3*, 199−249.
Abeygunawardana, C., Bush, C. A., & Cisar, J. O. (1990) *Biochemistry 29*, 234−248.
Biamonti, C., Rios, C. B., Lyons, B. A., & Montelione, G. T. (1994) *Adv. Biophys. Chem. 4*, 51−120.
Bonvin, A. M. J. J., & Brunger, A. T. (1996) *J. Biomol. NMR 7*, 72−76.
Borgias, B. A., & James, T. L. (1989) *Methods Enzymol. 176*, 169−183.
Brisson, J. R., & Carver, J. P. (1983) *Biochemistry 22*, 1362−1368.
Brisson, J. R., Baumann, H., Imberty, A., Perez, S., & Jennings, H. J. (1992) *Biochemistry 31*, 4996−5004.
Brooks, B. R., Bruccolerii, R. E., Olafson, B. D., States, D. J., Swaminathan, S., & Karplus, M. (1983) *J. Comput. Chem. 4*, 187−217.
Bruschweiler, R., Blackledge, M., & Ernst, R. R. (1991) *J. Biomol. NMR 1*, 3−11.
Bush, C. A. (1992) *Curr. Opin. Struct. Biol. 2*, 655−660.
Bush, C. A. (1994) *Methods Enzymol. 240*, 446−459.
Carver, J. P. (1993) *Pure Appl. Chem. 65*, 763−770.
Cassels, F., Hughes, C. V., & Nauss, J. L. (1995) *J. Ind. Microbiol. 15*, 176−185.
Cisar, J. O., Sanderberg, A. L., Abeygunawardana, C., Reddy, G. P., & Bush, C. A. (1995) *Glycobiology 5*, 655−662.
Cumming, D. A., & Carver, J. P. (1987) *Biochemistry 26*, 6676−6683.
de Waard, P., Leeflang, B. R., Vliegenthart, J. F., Boelens, R., Vuister G. W., & Kaptein, R. (1992) *J. Biomol. NMR 2*, 211−226.
Eberstadt, M., Gemmecker, G., Mierke, D. F., & Kessler, H. (1995) *Angew. Chem., Int. Ed. Engl. 34*, 1671−1695, and references cited therein.
Fesik, S. W., & Zuiderweg, E. R. P. (1988) *J. Magn. Reson. 78*, 588−593.
Gitti, R., Long, G., & Bush, C. A. (1994) *Biopolymers 34*, 1327−1338.
Gonzalez, C., Stec, W., Reynolds, M. A., & James, T. L. (1995) *Biochemistry 34*, 4969−4982.
Ha, S. N., Giammona, A., Field, M., & Brady, J. W. (1988) *Carbohydr. Res. 180*, 207−221.
Hamer, G. K., Balza, F., Cyr, N., & Perlin, A. S. (1978) *Can. J. Chem. 56*, 3109.
Homans, S. W. (1993) *Glycobiology 3*, 551−555.
Hricovini, M., Shah, R. N., & Carver, J. P. (1992) *Biochemistry 31*, 10018−10023.
James, T. L. (1991) *Curr. Opin. Struct. Biol. 1*, 1042−1053.
Jardetzky, O. (1980) *Biochim. Biophys. Acta 621*, 227−232.
Keepers, J. W., & James, T. L. (1984) *J. Magn. Reson. 57*, 404−426.
Kolenbrander, P. E., & London, J. (1993) *J. Bacteriol. 175*, 3247−3252.
Lommerse, J. P. M., Kroon-Batenburg, L. M. J., Kroon, J., Kamerling, J. P., & Vliegenthart, J. F. G. (1995) *J. Biomol. NMR 5*, 79−94.
Mierke, D. F., Scheek, R. M., & Kessler, H. (1994) *Biopolymers 34*, 559−563.
Miller, K. E., Mukhopadhyay, C., Cagas, P., & Bush, C. A. (1992) *Biochemistry 31*, 6703−6709.
Mulloy, B., Frenkiel, T. A., & Davies, D. B. (1988) *Carbohydr. Res. 184*, 39−46.
Podlaske, C. A., Wu, J., Stripe, W. A., Bondo, P. A., & Serianni, A. S. (1995) *J. Am. Chem. Soc. 117*, 8635−8644.
Poppe, L., & van Halbeek, H. (1992) *J. Am. Chem. Soc. 114*, 1092−1094.
Press, W. H., Teukolsky, S. A., Vetterling, W. T., & Flannery, B. R. (1992) *Numerical Recipes in C*, Cambridge University Press, Cambridge, U.K.
Reddy, G. P., Chang, C. C., & Bush, C. A. (1993) *Anal. Chem. 65*, 913−921.
Rice, K. G., Wu, P., Brand, L., & Lee,Y. C. (1993) *Curr. Opin. Struct. Biol. 3*, 669−674.
Rutherford, T. J., & Homans, S. W. (1994) *Biochemistry 33*, 9606−9614.
Rutherford, T. J., Neville, D. C., Homans, S. W. (1995) *Biochemistry 34*, 14131−7.
Saenger, W. (1983) *Principles of Nucleic Acid Structure* Springer-Verlag, Berlin.
Tvaroska, I., Hricovini, M., & Petrakova, E. (1989) *Carbohydr. Res. 189*, 359−362.
Ulyanov, N. B., Schimitz, U., Kumar, A., & James, T. L. (1995) *Biophys. J. 68*, 13−24.
van Gunsteren, W. F., Brunne, R. M., Gros, P., van Schaik, R. C., Schiffer, C. A., & Torda, A. E. (1994) *Methods Enzymol. 239*, 619−654.
Xu, Q. W., Mohan, S., & Bush, C. A. (1996a) *Biopolymers 38*, 339−353.
Xu, Q. W., Gitti, R., & Bush, C. A. (1996b) *Glycobiology 6*, 281−288.
Zhu, G., Renwick, A., & Bax, A. (1994) *J. Magn. Reson. A110*, 257−261.

BI961262+